Phase retrieval of images using Gaussian radial bases

Russell Trahan III* and David Hyland

Department of Aerospace Engineering—Texas A&M University, HRBB 701, Ross Street, TAMU 3141, College Station, Texas 77843, USA

*Corresponding author: rtrahan3@tamu.edu

Received 4 October 2013; revised 13 November 2013; accepted 13 November 2013; posted 14 November 2013 (Doc. ID 198842); published 11 December 2013

Here, the possibility of a noniterative solution to the phase retrieval problem is explored. A new look is taken at the phase retrieval problem that reveals that knowledge of a diffraction pattern's frequency components is enough to recover the image without projective iterations. This occurs when the image is formed using Gaussian bases that give the convenience of a continuous Fourier transform existing in a compact form where square pixels do not. The Gaussian bases are appropriate when circular apertures are used to detect the diffraction pattern because of their optical transfer functions, as discussed briefly. An algorithm is derived that is capable of recovering an image formed by Gaussian bases from only the Fourier transform's modulus, without background constraints. A practical example is shown.

OCIS codes: (070.6020) Continuous optical signal processing; (100.3190) Inverse problems; (100.5070) Phase retrieval; (110.2990) Image formation theory; (100.3175) Interferometric imaging; (110.3175) Interferometric imaging.

http://dx.doi.org/10.1364/AO.52.008627

1. Introduction

In the fields of imaging with application to astronomy and crystallography, phase retrieval has received much attention over the past decades, due to increases in computational power. The phase retrieval problem is a nonlinear estimation problem where the magnitude values of the Fourier transform of a 2D image are known but the phase values of the Fourier transform are unknown. The phase values must thus be estimated to recover the original image.

Many methods of phase retrieval are based on the work of Gerchberg and Saxton's error-reduction (ER) method [1]. The ER method is an iterative method that projects from the image domain to the Fourier domain and back, and imposes constraints upon each projection. Namely, the image is constrained to have real, positive pixel values and to have finite support. Thus, at every iteration some portion of the image is constrained to have zero pixel values. The Fourier domain of the image is constrained to have a modulus value equivalent to the given squared coherence data. It has been shown for many cases that iterative projections onto the two constrained spaces can provide a viable estimate of the missing phase. The algorithm, however, is notoriously susceptible to local minima in its error metric; i.e., it stagnates before converging to a reasonable estimate of the true image [2].

Fienup devised a modification called the hybrid input–output (HIO) method, where the image background constraint was modified [3,4]. Instead of rigidly constraining the background to have zero pixel values, a step is taken toward imposing the constraint based on the previous iteration's estimate. The result was a vast improvement over the ER method. The HIO method has become the field's standard method and the basis of comparison for most ongoing phase retrieval research.

Since the introduction of the ER and HIO methods, many additional modifications have been proposed to further increase the robustness of the estimator and to prevent stagnation. These modifications include

1559-128X/13/368627-07$15.00/0

estimation techniques for the background/support region as discussed in [5–7]. Much attention has been placed on the development of more creative gradient steps than what is used in the HIO method that can escape local minima [8], such as the difference map [9], averaged successive reflections [10], hybrid projection reflection [11], relaxed averaged alternating reflection [12], and constraint relaxation [13] to name a few. The inner workings of these methods are based on nonlinear estimation and function minimization techniques [14–17]. Explanations for the existence of the troublesome local minima have been offered, such as the existence of solutions convoluted with a mirror image of the solution [2]. Requirements have been formulated for the amount of oversampling required for 2D phase retrieval to have a unique solution [7]. Additionally, some papers have discussed the HIO method's performance and offered modifications for when the input Fourier modulus data suffers from low signal-to-noise levels [4,13,18–22].

In the fields of crystallography, x-ray diffraction imaging, and holography several approaches have been developed outside the HIO method's framework. Some methods, such as [23], use a CCD and a phase plate. This method is able to produce remarkable, experimentally validated results for arbitrary complex-valued images; however, its current application has only been demonstrated for very small length scales. Similarly, the discussions in [24] employ a mask and a CCD and produce very good results at small length scales. Many of these methods involve hardware and data collection methods not suitable for capturing astronomical bodies, as is the primary interest of the discussion here. Astronomical interferometry techniques often require baselines on the meter length scale and larger [25–27], which is not yet feasible for the aforementioned methods. Also, in the case for a body such as a rotating asteroid [28], multiple data records would not be practical as the object's appearance changes throughout time.

All of the methods based on the ER, HIO, and various projection methods, however, seem to suffer the same fates. Improved image resolution results in much longer computation times, since two fast Fourier transforms (FFTs) are performed at each iteration, each scaling as $N \log N$ for a dimension of the image having N pixels (exact scaling depends on the FFT algorithm but all have nonlinear growth with dimensionality). The Fourier domain measurements must be somewhat continuous, not sparse, which makes use of the HIO method in practical applications difficult. The HIO method and especially many of its variants have parameters that the user must adjust from one application to another, which adds some "art" to the process. In a truly blind test there is no definitive metric to determine whether the output image is correct or not. Finally, and most disconcertingly, because of the use of two FFTs in the algorithm iterations, there is very little possibility of an analytical solution to the phase retrieval problem existing within the ER or HIO frameworks.

In an attempt to overcome these several downfalls of HIO-based phase retrieval, the original concept of an image is revisited. In the HIO method, an image is thought of as a 2D, discrete array of numbers. This grid of numbers can be transformed from the image domain to the Fourier domain via a FFT; however, the question can be posed, "Why is everything treated as discrete?" If a better image has a higher resolution, i.e., smaller pixels, wouldn't the true image be continuous? This idea has led to research in the field of super resolution, which has its own set of challenges [29]. Here, a fresh look is taken with emphasis placed on maintaining continuity in the image rather than worrying about resolution. An image is considered continuous and any discrete representation of that image is a "sampling" of the continuous image. For this reason the use of pixels must be questioned [30].

To introduce this new look at phase retrieval, the continuous nature of an image, and how it can be sampled to be represented as discrete, is analyzed. Next, attention is transferred to an image's inherently continuous nature when a finite aperture is used for data acquisition. Finally, based on the insight of these discussions, a phase retrieval method is introduced that makes use of a continuous imaging framework and contains the potential for a noniterative phase solution for arbitrary geometries in images. An example using this new method is shown.

A. Pixels versus Gaussians

With modern computers, viewing, capturing, and editing images is extremely easy. Using some sort of graphics user interface (GUI), the user can edit pixel values across a 2D image with the click of a mouse. Often, the image is displayed in a manner that permits zooming to see the individual pixels and allow for precise editing. Upon zooming, almost all software represents pixels as squares that make up a grid, with each having a specific color value. Because the focus here is to create an image of a real object through phase retrieval of diffraction pattern information, the underlying concept of a digital image should be revisited.

If perfect data were acquired to represent a scene as an image, the resolution would be infinite and yield a continuous image. The image should, thus, be thought of as a continuous function in 2D space. In practice, this continuous function's value is only known at specific points, giving the need to interpolate to recover the original continuous image. Two of the most common techniques in computer graphics for changing the resolution of an image are nearest-neighbor and bilinear sampling [31–33].

Nearest-neighbor sampling assumes that the sampled value, $\hat{I}(x,y)$, is defined as

$$\hat{I}(x,y) = I(i,j), \qquad i = \text{round}(x), \qquad j = \text{round}(y), \tag{1}$$

where I is the true image function, $I(i,j)$ are the known image function values at integer coordinates, $(x,y) \in \Re^2$, and $(i,j) \in I^2$ [34]. The nearest-neighbor sampling technique of representing an image gives rise to the typical notion of having a rectilinear grid of squares as shown in the 1D example in Fig. 1. This is the method of image sampling most commonly used to formulate the phase retrieval problem because of the ease with which a 2D, discrete array of numbers, $I(i,j)$, can be discrete Fourier transformed. The major drawback to this method of sampling is that an analytical Fourier transform either does not exist or is far too cumbersome for arbitrary image functions. Additionally, nearest-neighbor sampling is known as the worst of the sampling techniques for representing images [34].

Bilinear sampling differs from nearest-neighbor sampling in that the sampled image stays continuous in its function value. Given image function values, $I(x,y)$, at integer positions (i,j) a bilinear interpolation is performed to obtain the image function values, $\hat{I}(x,y)$, in continuous (x,y) space in the form

$$\begin{aligned}\hat{I}(x,y) = {} & I(i^-,j^-)(i^+ - x)(j^+ - y) \\ & + I(i^+,j^-)(x - i^-)(j^+ - y) \\ & + I(i^-,j^+)(i^+ - x)(y - j^-) \\ & + I(i^+,j^+)(x - i^-)(y - j^-), \end{aligned} \tag{2}$$

where $i^- = \text{floor}(x)$ and $i^+ = \text{ceiling}(x)$, and likewise for j and y [34]. The bilinear interpolation is superior to nearest-neighbor sampling in terms of image quality, to a viewer. There is less visible evidence of the grid pattern due to the function's continuity across edges of grid elements, as shown in Fig. 1. A reason bilinear sampling is not advantageous to pursue in phase retrieval is, like nearest-neighbor sampling, there is no easy way to analytically Fourier transform an arbitrary image function.

Because neither nearest-neighbor nor bilinear sampling lends itself to analytical Fourier transformation, neither is really well suited for phase retrieval. A less common image reconstruction filtering technique is the Gaussian radial basis (GRB) function [30,35]. This technique places many 2D Gaussians across the image at specified positions and sums them to form a continuous, smooth image function. This image representation technique maintains not only continuity in the image function value but also in its slope. An analytical Fourier transform is also available. For this reason the GRB is enticing to use for phase retrieval. In the comparison in Fig. 1, six Gaussians are placed at $x = [0,1,2,3,4,5]$, with amplitudes $A = [1, 0.05, -0.95, -0.25, 1.05, 0.05]$ and standard deviation 0.5. The Gaussian interpolation matches the true function much more closely than the nearest-neighbor and linear interpolation. Additionally, Fig. 2 shows the image of a fictitious satellite formed with Gaussian bases. The blurring corresponds to the effect a finite aperture optical system would impose on the image, as will be discussed in the next section. While this does not prove that GRBs are superior, these examples demonstrate the concept of having an image with arbitrary geometries formed with Gaussians.

Why so much discussion of image sampling if the issue here is phase retrieval? Traditionally, phase retrieval algorithms treat the diffraction pattern information as discrete. To achieve better quality or higher resolution images in traditional phase retrieval, the resolution of the discrete map of the diffraction pattern is increased. Here, we will extract the diffraction pattern's continuous structure from the discrete measured data using a spectrum analysis, thus allowing for continuous functions throughout the phase retrieval process. The goal is to use discrete representations of information only if absolutely necessary and attempt to turn discrete, measured data into continuous information. Because an image must always be discretized before displaying to a computer monitor or printing, the continuous image function formed with GRBs can be sampled after the phase retrieval is performed.

B. Gaussians in Imaging

Another justification for using the GRB is that most data acquisition for imaging takes place using circular apertures. For a finite circular aperture, the point spread function has the form

$$U(\omega) = C\frac{J_1(\omega)}{\omega}, \tag{3}$$

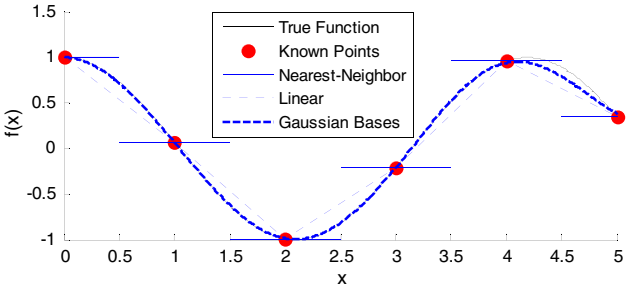

Fig. 1. Comparison of various sampling methods' representations of the function $\cos(x)$.

Fig. 2. Example image with arbitrary geometry formed with Gaussian bases.

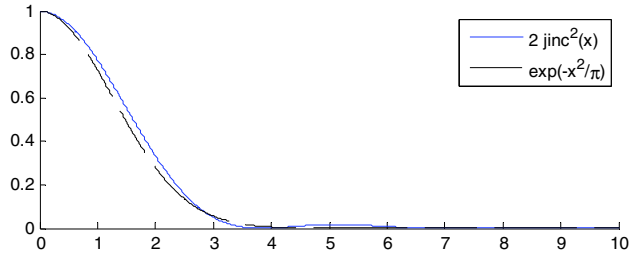

Fig. 3. Comparison of the jinc(x) function and a unit Gaussian approximation.

where $J_1(\omega)$ is the Bessel function of the first kind and C is a constant [36]. The intensity, called the Airy pattern, is thus

$$I(\omega) = C^2\left[\frac{J_1(\omega)}{\omega}\right]^2 = C^2[\text{jinc}(\omega)]^2. \tag{4}$$

The jinc function is often approximated as a Gaussian. As shown in Fig. 3, this approximation is accurate for most practical purposes and provides an easier expression for analytical work than the jinc function provides. Since the diffraction integral leads to a Gaussian (by approximation), the optical transfer function is also a Gaussian. This leads to the conclusion that all images viewed through a circular aperture are essentially formed by a network of Gaussians making the GRB image more representative of what an aperture captures than a pixelated image.

2. Phase Retrieval Using Gaussian Radial Bases

An image can be considered to be a function in 2D space, $I(\underline{\theta})$, where $\underline{\theta}$ is the spatial position vector. The image is the sum of N 2D Gaussians such that

$$I(\underline{\theta}) = \sum_{j=1}^{N} A_j \exp\left(-\frac{1}{2\sigma_j^2}(\underline{\theta} - \underline{\theta}_j)^2\right) \tag{5}$$

each having the amplitude A_j, location $\underline{\theta}_j$, and width σ_j. An image in this form has the continuous Fourier transform [37]

$$J(\underline{u}) = \sqrt{2\pi}\sum_{j=1}^{N} A_j\sigma_j \exp(-2\pi i\underline{u}\cdot\underline{\theta}_j)\exp(-2\sigma_j^2\pi^2\underline{u}\cdot\underline{u}), \tag{6}$$

based on the Fourier transform convention

$$J(\underline{u}) = \int_{-\infty}^{\infty} I(\underline{\theta})\exp(-2\pi i\underline{u}\cdot\underline{\theta})\mathrm{d}\underline{\theta}. \tag{7}$$

Often times in interferometry, the squared magnitude of the Fourier transform, also referred to as the squared coherence, is measured, thus making the squared coherence the input to the phase retrieval problem. Using the Gaussian bases, the squared coherence is

$$|J^2(\underline{u})| = \left|2\pi\sum_{j=1}^{N}\sum_{k=1}^{N}[A_jA_k\sigma_j\sigma_k \exp(-2\pi^2\sigma_j^2\sigma_k^2\underline{u}\cdot\underline{u}) \times \exp(-2\pi i\underline{u}\cdot(\underline{\theta}_j - \underline{\theta}_k))]\right|. \tag{8}$$

This expression leads to an interesting realization: the positions of the Gaussians in the image, $\underline{\theta}_j$ and $\underline{\theta}_k$, appear in the squared coherence expression as a frequency component in the Fourier domain. If the frequency components are identified, the relative positions of the Gaussians in the image can be determined.

To identify the frequency components within the squared coherence data, a Fourier transform (denoted the "spectrum analysis" $\hat{J}(\underline{\theta})$ for clarity) is performed such that

$$\hat{J}(\underline{\theta}) = F\{|J^2(\underline{u})|\}(\underline{\theta}) = \sqrt{2\pi}\sum_{j=1}^{N}\sum_{k=1}^{N} A_jA_k\frac{\sigma_j\sigma_k}{\sqrt{\sigma_j^2+\sigma_k^2}} \times \exp\left(-\frac{(\underline{\theta}+\underline{\theta}_j-\underline{\theta}_k)^2}{2(\sigma_j^2+\sigma_k^2)}\right). \tag{9}$$

The spectrum contains N^2 Gaussians translated across the $\underline{\theta}$ space; however, N of the Gaussians are at the origin. This means there are $N(N-1)$ unique Gaussians. The translations of the Gaussians reveal a useful property. Consider a single value of j. For all k, the image's Gaussians are placed such that the entire image is revealed with the $j = k$ Gaussian at the origin. This realization reveals the fact that the true image occurs N times in the spectrum, with each instance of the image translated such that one of the Gaussians is at the origin.

Since the measured squared coherence data is typically discrete, a discrete Fourier transform can be performed that will reveal local maxima indicating each frequency component. Additionally, a Gaussian can be fitted at each local maxima to identify the standard deviation and amplitude of the Gaussian. Because the frequency components, amplitudes, and standard deviations of the continuous image can be determined from the discrete squared coherence data, a transition can be made from discrete to continuous. Ideally, there are $N(N-1)$ maxima. A problem can occur if multiple $\underline{\theta}_j - \underline{\theta}_k$ pairs have the same value. This would cause the Gaussians in the spectrum to overlap, thus masking the two Gaussians as one larger Gaussian. This problem has not yet been solved. For multiple $\underline{\theta}_j - \underline{\theta}_k$ pairs close in value, but not equal, the two summed Gaussians in the spectrum may present a case where the Gaussians overlap enough that only one local maxima exists. In this case, rather than searching for local maxima, a Gaussian based fitting method could produce the proper results. This idea has not been fully investigated yet but may prove more accurate than simply locating local maxima.

Fig. 4. Sample image for the algorithm demonstration.

Algorithm 1, shown below, can be used to identify the N overlapping images. The goal here is to add one Gaussian to the image estimate at a time, making sure the Gaussian added belongs to the main image instance and not one of the translated instances. The image is built up one Gaussian at a time until the true image is revealed.

Figure 4 shows a simple image with four Gaussians. The spectrum analysis of this image is shown in Fig. 5, which contains the four translated images. The bold arrows show the development of the main image instance. The lighter arrows show the development of the secondary translated images, each with different dashed lines. Note that any of the translated images shown could be considered the main image, depending upon the algorithm's starting choice.

Once the individual Gaussians in the image are found, the image can be reconstructed using Eq. (5). The resulting image is continuous and has infinite extents. The image function can be nearest-neighbor-sampled to create a grid of discrete pixel values for display.

Algorithm 1. Image Reconstruction from Spectrum Analysis.

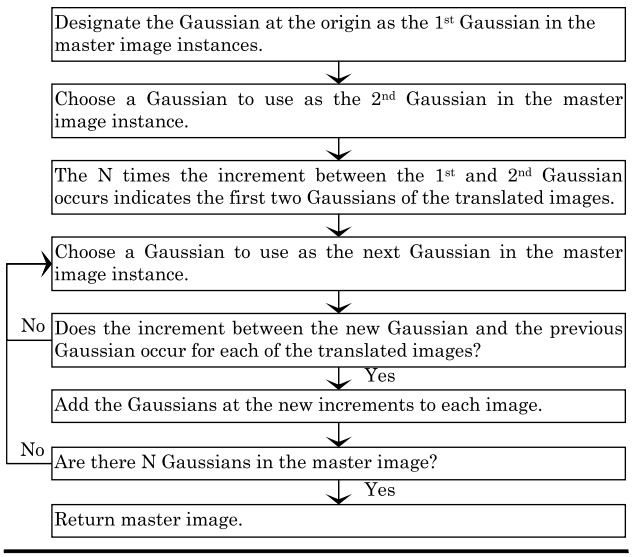

3. Example in Astronomy

To demonstrate this technique of phase retrieval, consider the Pleiades star cluster shown in Fig. 6.

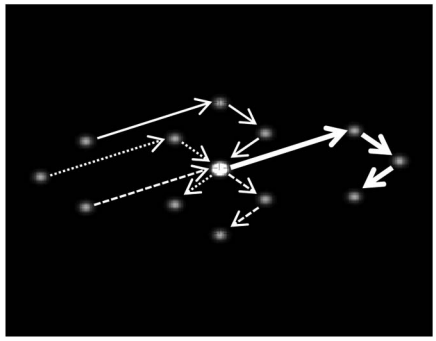

Fig. 5. Sample image spectrum analysis showing the progressive development of the four translated images. Each image has different line styles connecting the four Gaussians in the order that Algorithm 1 identified the Gaussians.

For the sake of this example, the image was created such that it can be represented as a continuous function with nine Gaussians representing the nine main stars in the cluster. The measured squared coherence data in Fig. 7, sampled from the continuous Fourier transform of the image, has a resolution of 1024×1024. The spectrum analysis shown in Fig. 8 is merely the discrete Fourier transform of this 1024×1024 array.

The spectrum was scanned to find all of the positions, widths, and amplitudes of the Gaussians that are then used in the phase retrieval algorithm.

Fig. 6. Pleiades star cluster used as an example of GRB phase retrieval; this image serves as both of the inputs to the phase retrieval algorithm.

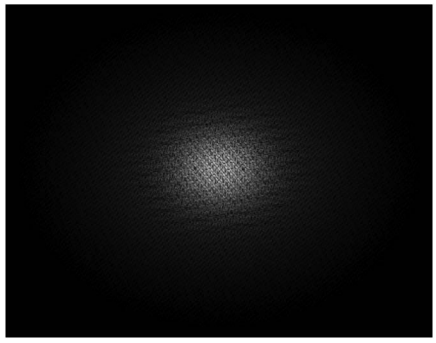

Fig. 7. Squared Fourier modulus of the Pleiades star cluster image represented as a 1024×1024 array.

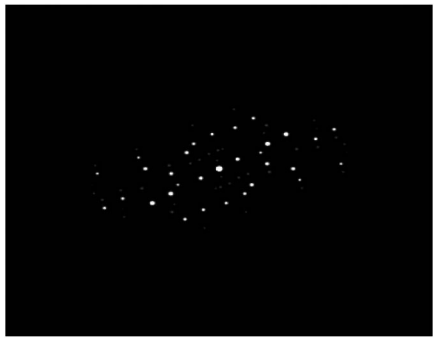

Fig. 8. Spectrum analysis of the Fourier transform of the Pleiades image.

Fig. 9. Estimated image of the Pleiades resulting from the application of Algorithm 1 to the spectrum analysis in Fig. 8. The continuous image is point sampled for display.

The resolution of the measured squared coherence data dictates the resolution of the spectrum, which limits the accuracy when determining the positions of the Gaussians in the spectrum. This limited accuracy in turn limits the accuracy of the final image. The result of Algorithm 1 is shown in Fig. 9. The positions of the Gaussians in the final image are accurate to $\pm 1/2$ pixel.

It is also worth mentioning that the HIO method can be used to obtain the phase estimate for this image. The HIO method, with feedback parameter $\beta = 0.9$ and proper rectangular background constraints, requires approximately 500 iterations to converge to nearly zero error. For this image, with resolution 512×512, the stars are not well defined, due to the pixilation. The reproduced image in Fig. 10 looks fine; however, upon closer inspection, near one of the stars there is much distortion. A comparison is shown in Fig. 11 between the topmost star in the GRB image and the HIO image. In the discrete HIO image the star is not perfectly round, and there is no clear metric for describing the radius of the star. The Gaussian bases, however, give a clear metric: the standard deviation of the continuous Gaussian. Note that the GRB allows for a discrete image to be produced at any resolution because it is a continuous image.

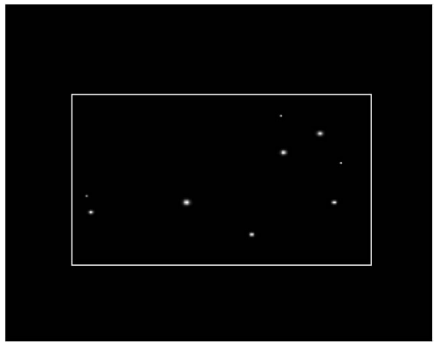

Fig. 10. 512×512 pixel result from the HIO method with a rectangular support region.

(a) GRB Result (b) HIO Result

Fig. 11. Topmost star in the (a) GRB and (b) HIO images as shown in Figs. 9 and 10, respectively.

4. Conclusions

A notable benefit of use of the spectrum analysis of the squared coherence data over directly inverse Fourier transforming, as is the case in the HIO method, is that the Fourier domain must only contain enough measurements to identify its frequency components. Traditional phase retrieval methods require either complete Fourier domain coverage via measurements or some kind of estimation of the missing data. There are potentially other methods of identifying these frequency components beyond the discussion here that may lead to more accurate results and can tolerate the overlapping frequency components, as discussed earlier. An additional benefit of this spectrum analysis method is the inherent continuity of the image. As shown in the HIO results, pixilation can alter the content of the image. In the example shown, due to the pixilation, a round star doesn't appear round and the boundaries of the star are vague.

In practice, the measured squared coherence data contains some amount of noise that causes a lack of smoothness in the Fourier domain. Because the Fourier transform of the coherence data is used to generate the spectrum, the smoothing effect of the Fourier transform helps to alleviate the effect of noise. Since this method of phase retrieval is in its infancy, no explicit noise analysis has been performed yet.

The method presented here builds upon the successes and shortcomings of prior research in the phase retrieval field, but also takes a step back and approaches the problem from a new point of view. The properties of finite aperture optics and the continuity of an image viewed through a finite aperture lead to the Gaussian bases. The algorithm

presented here employs a recursive scheme to find each Gaussian in the image based on the pattern in the spectrum analysis. This algorithm is not iterative in the sense that there are a fixed number of recursions needed to resolve the image. This contrasts with the HIO method and other projective methods. In these other methods, a subsequent iteration can always be performed and, in theory, every subsequent iteration gives a better estimate of the image. Here, once the correct pattern is found via recursion, a closed form equation relates the Gaussian locations in the spectrum analysis with the bases of the image.

Ongoing work on this topic includes improvement to the spectrum analysis to allow for images with many more Gaussians than the example shown here and a quantification of the effect of noise on this algorithm.

References

1. R. W. Gerchberg and W. O. Saxton, "A practical algorithm for the determination of the phase from image and diffraction plane pictures," Optik **35**, 237–250 (1972).
2. J. R. Fienup and C. C. Wackerman, "Phase-retrieval stagnation problems and solutions," J. Opt. Soc. Am. A **3**, 1897–1907 (1986).
3. J. R. Fienup, "Phase retrieval algorithms: a comparison," Appl. Opt. **21**, 2758–2769 (1982).
4. J. R. Fienup, "Reconstruction of an object from the modulus," Opt. Lett. **3**, 27–29 (1978).
5. J. S. Wu, U. Weierstall, and J. Spence, "Iterative phase retrieval without support," Opt. Lett. **29**, 2737–2739 (2004).
6. S. Marchesini, H. He, H. N. Chapman, S. P. Hau-Riege, A. Noy, M. R. Howells, U. Weierstall, and J. Spence, "X-ray image reconstruction from a diffraction pattern alone," Phys. Rev. B **68**, 140101 (2003).
7. J. Miao, D. Sayre, and H. N. Chapman, "Phase retrieval from the magnitude of the Fourier transforms of nonperiodic objects," J. Opt. Soc. Am. A **15**, 1662–1669 (1998).
8. S. Marchesini, "A unified evaluation of iterative projection algorithms for phase retrieval," Rev. Sci. Instrum. **78**, 011301 (2007).
9. V. Elser, "Phase retrieval by iterated projections," J. Opt. Soc. Am. A **20**, 40–55 (2003).
10. H. H. Bauschke, P. L. Combettes, and D. R. Luke, "Phase retrieval, error reduction algorithm, and Fienup variants: a view from convex optimization," J. Opt. Soc. Am. A **19**, 1334–1345 (2002).
11. H. H. Bauschke, P. L. Combettes, and D. R. Luke, "Hybrid projection–reflection method for phase retrieval," J. Opt. Soc. Am. A **20**, 1025–2034 (2003).
12. D. R. Luke, "Relaxed averaged alternating reflections for diffraction imaging," Inverse Probl. **21**, 37–50 (2005).
13. R. Trahan and D. Hyland, "Mitigating the effect of noise in the hybrid input–output method of phase retrieval," Appl. Opt. **52**, 3031–3037 (2013).
14. S. Babaoe-Kafaki, "A quadratic hybridization of Polak–Ribière–Polyak and Fletcher–Reeves conjugate gradient methods," J. Optim. Theory Appl. **154**, 916–932 (2012).
15. R. Fletcher and C. Reeves, "Function minimization by conjugate gradients," Comput. J. **7**, 149–154 (1964).
16. E. Polak, "Computational methods in optimization; a unified approach," Math. Program. **3**, 131–133 (1972).
17. E. Polak and G. Ribiére, "Note sur la convergence de méthodes de directions conjuguées," Rev. Fr. Inf. Rech. Oper. **3**, 35–43 (1969).
18. G. Liu, "Fourier phase retrieval algorithm with noise constraints," Sig. Process. **21**, 339–347 (1990).
19. G. Liu, "Object reconstruction from noisy holograms: multiplicative noise model," Opt. Commun. **79**, 402–406 (1990).
20. R. Bates and D. Mnyama, "The status of practical Fourier phase retrieval," *Advances in Electronics and Electron Physics* (Academic, 1986), Vol. **67**, pp. 1–64.
21. M. Kohl, A. A. Minkevich, and T. Baumback, "Improved success rate and stability for phase retrieval by including randomized overrelaxation in the hybrid input output algorithm," Opt. Express **20**, 17093–17106 (2012).
22. G. Williams, M. Pfeifer, I. Vartanyants, and I. Robinson, "Effectiveness of iterative algorithms in recovering phase in the presence of noise," Acta Crystallogr. A **63**, 36–42 (2007).
23. F. Zhang, G. Pedrini, and W. Osten, "Phase retrieval of arbitrary complex-valued fields through aperture-plane modulation," Phys. Rev. A **75**, 043805 (2007).
24. W. Chen and X. Chen, "Quantitative phase retrieval of complex-valued specimens based on noninterferometric imaging," Appl. Opt. **50**, 2008–2015 (2011).
25. R. Hanbury Brown and R. Q. Twiss, "A new type of interferometer for use in radio astronomy," Philos. Mag. **45**(7), 663–682 (1954).
26. R. Hanbury Brown and R. Q. Twiss, "A test of a new type of Stellar Interferometer on Sirius," Nature **178**, 1046–1048 (1956).
27. R. Hanbury Brown and R. Q. Twiss, "Interferometry of the intensity fluctuations in light," Proc. R. Soc. B **242**, 300–324 (1957).
28. H. Altwaijry and D. Hyland, "Detection and characterization of near Earth asteroids using stellar occultation," in *AAS/AIAA Astrodynamics Specialist Conference*, Hilton Head, South Carolina, 2013.
29. E. Gur, V. Sarafis, I. Falat, F. Vacha, M. Vacha, and Z. Zalevsky, "Super-resolution via iterative phase retrieval for blurred and saturated biological images," Opt. Express **16**, 7894–7903 (2008).
30. A. R. Smith, "A pixel is not a little square," *Microsoft Technical Memo 6* (Microsoft, 1995).
31. R. Fernando, *GPU Gems: Programming Techniques, Tips and Tricks for Real-Time Graphics* (Pearson Higher Education, 2004).
32. M. Pharr and R. Fernando, *GPU Gems 2: Programming Techniques for High-Performance Graphics and General-Purpose Computation* (Addison-Wesley, 2005).
33. P. S. Heckbert, "Survey of texture mapping," IEEE Comp. Grap. Appl. **6**, 56–67 (1986).
34. D. Shreiner, G. Sellers, J. M. Kessenish, and B. M. Licea-Kane, *OpenGL Programming Guide* (Addison-Wesley, 2013).
35. E. Hartman and J. Keeler, "Layered neural networks with Gaussian hidden units as universal approximations," Neural Comput. **2**, 210–215 (1990).
36. M. Born and E. Wolf, *Principles of Optics*, 6th ed. (Cambridge University, 1997).
37. M. Abramowitz and I. A. Stegun, *Handbook of Mathematical Functions with Formulas, Graphs, and Mathematical Tables* (Dover, 1964).